Applied Catalysis B: Environmental 237 (2018) 1021–1032

Contents lists available at ScienceDirect

Applied Catalysis B: Environmental

journal homepage: www.elsevier.com/locate/apcatb

Three-way catalysis with supported gold catalysts: Poisoning effects of hydrocarbons

Viktor Ulrich[a], Christian Froese[a,b], Boris Moroz[c,d], Pavel Pyrjaev[c], Evgeny Gerasimov[c,d], Ilya Sinev[e], Beatriz Roldan Cuenya[e,f], Martin Muhler[a], Valerii Bukhtiyarov[c,d], Wolfgang Grünert[a,*]

[a] Lehrstuhl Technische Chemie, Ruhr-Universität Bochum, D-44780 Bochum, Germany
[b] Max-Planck-Institut für Chemische Energiekonversion, D-45470 Mülheim (Ruhr), Germany
[c] Boreskov Institute of Catalysis, Novosibirsk 630090, Russian Federation
[d] Novosibirsk State University, Novosibirsk 630090, Russian Federation
[e] Experimentalphysik IV, Ruhr-Universität Bochum, D-44780 Bochum, Germany
[f] Fritz-Haber-Institut der Max-Planck-Gesellschaft, D-14195 Berlin, Germany

ARTICLE INFO

Keywords:
Au
TWC deactivation
TWC regeneration
Active support oxygen
In-situ DRIFTS

ABSTRACT

Poisoning phenomena recently observed during the conversion of three-way catalysis model feed (CO, NO propene, O_2, without or with water) over supported Au catalysts [V. Ulrich et al., Applied Catalysis B 203 (2017) 572] were investigated by reaction studies (replacing propene by propane in model feed, study of CO oxidation without and with relevant additional components), by temperature-programmed oxidation of deposits (TG, TPO), by studying self-regeneration phenomena and by DRIFTS of CO adsorption and co-adsorption of CO and propene under different conditions. During CO oxidation in the presence of other components, two different poisoning phenomena were observed. In the presence of propane, propene, and/or NO, CO oxidation was significantly inhibited below 370 K over Au on Al_2O_3 or on La-stabilized Al_2O_3, but not on Au/$CeZrO_x$ where activity was relatively low anywhere. DRIFTS data on (co-)adsorption of CO and propene suggest that this poisoning is not merely a result of site blocking by the coadsorbate, but that electron transfer from the co-adsorbates towards the active sites, which are assumed to be at the perimeter of positively charged Au clusters with the support, might have additionally quenched the reaction. At higher temperatures, a different poisoning mechanism operates in propene-containing mixtures. From studies by TPO, TG, and DRIFTS, we conclude the formation of carbonaceous residues, which do not block, however, CO adsorption sites but the support surface around Au clusters instead. While this inhibits CO oxidation involving active support oxygen, the same oxygen species might combust the deposits at higher temperatures. This results in self-regeneration phenomena depending on the redox activity of the support, the temperature and the propene content in the feed. In transient experiments, it was observed that NO is most favorably reduced by intermediates of coke formation from propene. Under stationary conditions, however, NO reduction, mostly by CO, remains insufficient.

1. Introduction

Since the 1970s the three-way catalyst (TWC) has become an important component of all gasoline-driven cars aiming at the attenuation of their environmental impact [1]. It converts the harmful exhaust components CO, unburned hydrocarbons (HC), and NO_x (NO and NO_2) into the harmless compounds CO_2, N_2, and H_2O. To catalyze these reactions, the TWC contains Pt, Pd, and Rh in different combinations supported on refractive oxides with high surface area (e.g. γ-Al_2O_3, ZrO_2, stabilized against sintering by La or Ba additives), or on oxygen storage compounds (usually Ce-Zr mixed oxides) [2]. Operation at low temperatures, e.g. during the cold start phase or under idling conditions, is a sore point with present-day TWCs, which has been addressed by a number of secondary approaches (traps, close-coupled converters) [3]. However, further improvement of the TWC itself is also desirable to solve this problem more directly. Including gold into TWC formulations is an interesting approach along this line. The idea has been part of critical discussions [4–6].

In 2002, application of a supported Au catalyst in three-way catalysis was first reported in the open literature by Mellor et al. [7]. The

* Corresponding author at: Lehrstuhl Technische Chemie, Ruhr-Universität Bochum, P. O. Box 102148, D-44780 Bochum, Germany.
E-mail address: w.gruenert@techem.ruhr-uni-bochum.de (W. Grünert).

https://doi.org/10.1016/j.apcatb.2018.06.063
Received 10 April 2018; Received in revised form 21 June 2018; Accepted 25 June 2018
Available online 26 June 2018
0926-3373/ © 2018 Elsevier B.V. All rights reserved.

authors deposited gold on a complex support comprising ZrO_2-stabilized CeO_2, ZrO_2, and TiO_2 and promoted with Co oxides, ZnO_x, MgO, BaO, and Rh. Under reducing conditions, this catalyst fully oxidized CO, propane, and propene and reduced NO, though at rather high temperature: light-off temperatures T_{50} (Temperature of 50% conversion) were reported to be ≈573 K with Rh added, and 653 K without Rh. Under oxidizing conditions, NO reduction did not reach even 50% conversion [7]. We have recently examined monometallic Au supported on γ-Al_2O_3, La-stabilized Al_2O_3, TiO_2, and Ce-ZrO_x for its behavior in three-way catalysis [8]. The choice of these supports was motivated by the composition of real TWCs (see above) and by the tremendous role of Au/TiO_2 in recent research on low-temperature CO oxidation. CO conversion was fast on these catalysts, whereas NO reduction remained insufficient over all of them. In the model feed containing CO together with propene, NO, and oxygen, CO oxidation was strongly attenuated, with light-off temperatures far above those observed in a binary CO/O_2 feed. Propene was proposed to poison CO oxidation in this feed. Its poisoning efficiency strongly depended on the water content in the feed and on the nature of the support, being most pronounced under dry conditions and on non-reducible supports. In the present paper we report more evidence on the nature of the poisoning of CO oxidation during three-way catalysis over supported Au catalysts, in particular on its origin and on opportunities to alleviate the effect.

2. Experimental

2.1. Catalyst preparation

Details of catalyst preparation have been reported recently [8]. Al_2O_3, La-stabilized Al_2O_3, and a ceria-zirconia mixed oxide, which will be denoted as "$CeZrO_x$" were used as supports for gold deposition. $CeZrO_x$ was donated by Umicore & Co. KG Hanau (Germany). Both alumina-based supports were supplied by Sasol Germany GmbH (Puralox SCFa 140 and SCFa 140-L3), supplier information about composition is given in the supporting information. Gold (1.6–1.8 wt-%) was deposited on these supports by a version of the deposition-precipitation route, where an aqueous Au solution obtained by neutralization of $HAuCl_4$ (Aurat, Russia, chemically pure) with NaOH (Reakhim, Russia, analytical grade) was added to a dried support at 343 K [9,10]. After washing, the resultant material was dried in vacuo and calcined in air at 573 K for 4 h. Exact compositions and texture data of these catalysts as well as surface compositions derived from XPS can be found in Ref. [8].

2.2. Catalyst characterization

After catalytic runs, the texture of the catalysts and the dispersion of Au particles were studied by nitrogen physisorption and by Transmission Electron Microscopy (TEM). The physical surface area was determined after degassing at 473 K using a Quantachrome Autosorb-1-MP and applying the BET model. Pore volume and pore size distributions were obtained following the BJH method. Electron microscopy was performed with a JEM-2010 (JEOL, Japan), which offers a lattice resolution of 0.14 nm at 200 kV accelerating voltage. Mean Au particle diameters were derived counting more than 300 particles in micrographs.

Deposits after catalysis were also examined by Temperature Programmed Oxidation (TPO) and by Thermogravimetry. TPO was made in an 80 mL min^{-1} flow of 5% O_2/He raising the temperature to 973 K at a rate of 5 K min^{-1}. Measured CO, CO_2 and N_2O concentrations were converted in amounts (μmol) released per g catalyst according to Eq. (1) (c_i – concentration of component i / ppm, V_m - molar volume under standard condition (24.465 L mol^{-1}), m_{cat} – catalyst mass / g, $\dot{V}$ – flow rate / L min^{-1})

$$n_i = \frac{\int_{t_0}^{t} c_i \, dt}{m_{cat}} \bullet \left(\frac{\dot{V}}{V_m} \right) \quad (1)$$

In addition, thermogravimetric analysis (TGA) of deposits was made using a Cahn TG 2131 thermobalance equipped with a quadrupole mass spectrometer. Spent catalysts (ca. 40 mg) were heated in a 100 mL min^{-1} flow of 20% O_2/He up to 900 K with a rate of 5 K min^{-1}.

Adsorption of CO on the supported Au catalysts and the influence of propene on it were investigated by low-pressure (co-)adsorption experiments monitored by Diffuse Reflectance Infrared Fourier Transform Spectroscopy (DRIFTS). The study was performed with a Nicolet *NEXUS*™ FT-IR spectrometer equipped with a liquid-nitrogen cooled *MCT-A detector* and an *Ever-Glow* mid-IR source and using a *PIKE DiffuseIR*™ diffuse reflectance accessory with a *PIKE DiffuseIR*™ high-temperature environmental chamber equipped with KBr windows. A home-built pressure control system employing a turbomolecular pump and an electronically actuated leaking-valve was connected to the environmental chamber. It allowed evacuation of the measurement chamber to a base-pressure of $2 \cdot 10^{-6}$ mbar and adjustment of constant probe molecule pressure up to 100 mbar.

Ca. 30 mg of the finely ground catalysts were placed in a reaction crucible made of a porous ceramic. Sample pretreatment was performed at 523 K (heating ramp β = 5 K min^{-1}) for 2 h in high-vacuum. After cooling the samples to 303 K, the measurement chamber was evacuated until base-pressure and background spectra were collected at a spectral resolution of $\Delta\nu = 4\ cm^{-1}$ (256 scans, aperture setting of 150). Commercial software (OMNIC) was used for background subtraction and data evaluation. All spectra of adsorbed probe molecules will be reported in terms of the pseudo-absorbance (log(1/R), R – reflectance of the sample) because for strongly absorbing materials such as oxide-supported metals, this quantity gives a more linear representation of band intensities *vs.* the surface coverage of the absorbing species than the Kubelka-Munk function [11].

Adsorption of CO was performed on pretreated samples at 303 K with stepwise increased pressures starting from high vacuum, with immediate begin of data collection after adjustment to desired pressures. Co-adsorption was studied analogously with propene and CO mixed at a ratio of 1:9. At each pressure setting, conditions were kept constant over time until there were no further changes in the spectra (typically 60 min). For Au/La-Al_2O_3, the influence of propene on the adsorption of CO was also examined at elevated temperature (423 K). Details will be given in Section 3.2.6.

2.3. Catalytic studies

All catalytic experiments were performed in a catalytic microflow reactor (a vertical V4A stainless steel tube with 14 mm inner diameter heated by a tubular furnace) at atmospheric pressure at temperatures between 323 and 673 K with a temperature ramp of 5 K min^{-1} as described in more detail elsewhere [8]. A total flow rate of 183 mL min^{-1} was fed over quartz-diluted 125 mg catalyst resulting in a gas-hourly space velocity (GHSV) of 60,000 h^{-1}.

For *Three-way catalysis,* three alternative stoichiometric model feeds were employed, in which the model hydrocarbon was propene, propane, or absent. They consisted of CO (1.1%), NO (0.1%), propane or propene (0.1% if present), O_2 (with propane – 1.0%, with propene – 0.95%, without hydrocarbon – 0.5%), and He (balance). Aiming at the elucidation of a poisoning mechanism, we have opted for dry feeds despite their lower technical relevance because hydrocarbon poisoning is more intense in the absence of water [8]. In the following, we will refer to the feed containing hydrocarbon as "TWC feed", to the one without hydrocarbons as "HC-off" feed. On-line analysis of all products was performed by combining a calibrated mass spectrometer (for O_2, NO, propene, propane) and a non-dispersive IR photometer (for CO, CO_2, N_2O). Conversions of CO, NO, and propane or propene were

calculated according to Eq. (2) (example −CO; index 0 – initial)

$$X_{CO} = (c_{CO,0} - c_{CO})/c_{CO,0} \quad (2)$$

Formation of N_2O will be reported as ppm content in the effluent. Light-off temperatures T_{50} will be used to compare catalyst activities.

CO oxidation in a stoichiometric mixture (CO (1.1%), O_2 (0.55%), balance He) was used to probe activity of partially poisoned Al_2O_3-, La-Al_2O_3- and $CeZrO_x$-based catalysts. For this purpose it was performed at 423 K, which is high enough to expect near 100% conversion over the fully active Au if supported on La-Al_2O_3 or $CeZrO_x$, and ca. 50% for Au/Al_2O_3 (cf. Fig. 3), but low enough to avoid drastic impact on the deposits. To further confine the latter, conversions were registered after just 10 min time on stream. In a typical regeneration experiment, the catalyst was poisoned by heating it in the TWC feed to 423 K. Subsequently, it was treated in He at different temperatures between 473 K and 623 K and kept there for 1 h before cooling to 423 K in He for probing the CO oxidation activity.

In some cases, *CO oxidation* was studied also *in the presence of hydrocarbon* (i.e. without NO). In these experiments, feeds consisted of CO (1.1%), 0.1% of the hydrocarbon, O_2 (1.0% for propene, 1.05% for propane), and He. All the mixtures (including the HC-off feed) were stoichiometric, but their O_2 content varied to some extent depending on the content of oxidizable components and NO. It will be seen below that changes of reaction rates by the poisoning effects were much larger than variations expected from influences of O_2 concentration via a kinetic rate law.

The hydrocarbon-free feed was also examined with respect to its potential to regenerate the catalyst. In these "*feed variation experiments*", which turned out to reveal instructive transient phenomena, the catalysts were charged alternatively with two stoichiometric feeds containing either propene ("TWC feed") or no hydrocarbon ("HC-off") at 423 K, 523 K, and 673 K. After this first sequence, they were oxidized in 2% O_2/He for 30 min at 673 K to remove deposits, then the sequence was repeated. Subsequently, the catalysts were cooled in He and deposits were examined in TPO or TG (see above). The scheme of the feed variation experiment is shown for reference in Fig. S1 (supporting information).

3. Results and discussion

3.1. Textural and Au dispersion in spent catalysts

Data on texture and Au particle size after one sequence of the feed variation experiment with final catalyst reoxidation is summarized in Table 1. The most severe part of the procedure experienced by the catalysts is exposure to the dry feed for about 50 min followed by oxidation in 2% O_2/He for 30 min, all at 673 K (Fig. S1). This caused the number-weighted average Au particle size to increase by a factor of ≈1.5. There is also a slight decrease of BET surface area and pore volume, for the BET surface area more pronounced with the alumina-based supports than with $CeZrO_x$. Neither texture nor Au particle size changed significantly during a second feed variation sequence. The particle size of Au on the Al_2O_3-based catalysts remained significantly lower than for Au on $CeZrO_x$.

The initial oxidation state of gold was zero in these catalysts as evidenced by our previous XPS measurements [8]. We do not expect this to have changed by use in TWC as alumina-supported Au has been shown recently to stay in the metal state even after thermal treatment in an oxidative atmosphere (selective reduction of NO by hydrocarbons in 10% O_2 at temperatures) up to 723 K [12].

3.2. Reaction studies

3.2.1. Three-way catalysis with propane and propene: a comparison

The huge poisoning effects on CO oxidation in TWC model feed assigned to propene in our previous work [8] raised the question if propene could represent all hydrocarbons with respect to its poisoning efficiency or if it is special because of a particular reactivity of its double bond towards the CO oxidation sites. Therefore, the behavior of supported Au catalysts in a feed containing propane instead of propene was examined. Results are summarized in Fig. 1 and Table 2. N_2O formation is included as an inset in Fig. 1c.

With propane representing the unburned hydrocarbon, CO was completely converted over all Au catalysts below 600 K (Fig. 1a). Light-off temperatures were again influenced by the nature of the support, but the differences were less drastic than with propene in the feed. With propane, T_{50} was highest for Au/Al_2O_3 (≈ 535 K), lower for Au/$CeZrO_x$ (≈ 430 K) and lowest for Au/La-Al_2O_3 (≈ 415 K). Notably, ranking between Au on La-Al_2O_3 and $CeZrO_x$ was reverted by the choice of the hydrocarbon (Table 2). The dependence of light-off temperatures on the hydrocarbon was weak over Au/$CeZrO_x$, but very strong for the other two catalysts.

Propane conversions did not exceed 30% in the whole temperature range up to 750 K (Fig. 1b), which differs drastically from propene conversions in propene-containing feed [8]. The smaller reactivity of Au towards propane than towards propene is also documented in the light-off temperatures collected in Table 2. These observations are in good agreement with recent literature [13,14]. Closer inspection shows some interesting details highlighting differences in the influence of the supports on gold. Over Au/$CeZrO_x$, propane conversion increased up to 500 K but decreased again upon further raising temperature up to 650 K (Fig. 1b). The simultaneous peaks in NO conversion and N_2O formation (Fig. 1c) suggest that NO is reduced by propane between 450 and 600 K, N_2O being the main product. A similar NO conversion to N_2O can be noted also for Au/La-Al_2O_3, though at lower temperature and stopping suddenly below 500 K (Fig. 1c). This feature is, however, not associated with an obvious propane conversion peak (Fig. 1b), instead, CO conversion increased more steeply in this temperature range than in the case of Au/$CeZrO_x$ (Fig. 1a). Thus, the minor differences between the CO conversion curves of these two catalysts between 400 and 470 K are no artifact, but indicate that NO was reduced predominantly by propane over Au/$CeZrO_x$ and by CO over Au/La-Al_2O_3. Over Au/Al_2O_3, NO was not at all affected below 750 K.

From a more general viewpoint, the performance of gold catalysts

Table 1
Metal loadings (X-ray Fluorescence, from Ref. [8].), textural data (BET/BJH) and number-weighted average particle sizes d_l (TEM) of fresh and spent Au catalysts.

Catalyst	Au, wt%	Average particle diameter $< d_l \pm \sigma >$ [a], nm	BET surface area, m^2g^{-1}	Mean pore diameter, nm	Pore volume, $cm^3\ g^{-1}$
Au/Al_2O_3 Fresh[b]	1.8	1.5 ± 0.3	150	11.7	0.44
Spent[c]	–	2.5 ± 0.6	129	12.0	0.38
Au/La-Al_2O_3 Fresh[b]	1.8	1.7 ± 0.3	135	13.3	0.45
Spent[c]	–	2.2 ± 0.5	120	13.4	0.41
Au/$CeZrO_x$ Fresh[b]	1.6	2.8 ± 0.6	65	14.8	0.24
Spent[c]	–	4.1 ± 0.9	59	13.8	0.20

[a] $d_l = \Sigma d_i/N$, where d_i – Au particle diameter, N – total number of particles observed, σ- standard deviation.
[b] From Ref. [8].
[c] Aged by feed variation experiment, see end of Section 2.3.

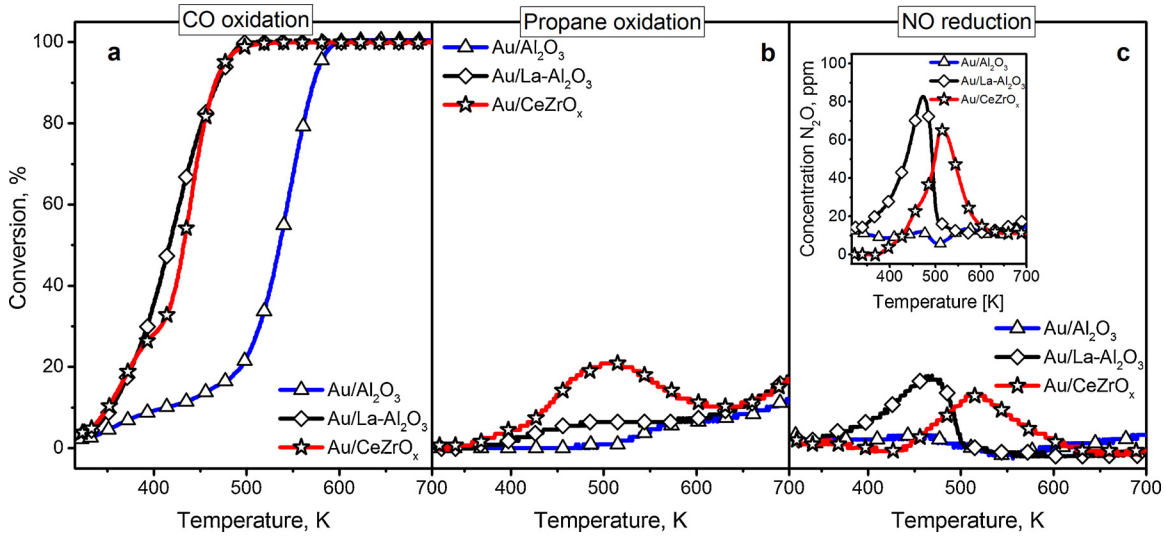

Fig. 1. Temperature dependence of CO, propane, and NO conversions in a stoichiometric dry model feed over Au/Al_2O_3 (blue, triangle), $Au/La\text{-}Al_2O_3$ (black, diamond) and $Au/CeZrO_x$ (red, star). N_2O formation is shown as an inset in c). Prior to these runs, the catalysts were used in one run of stoichiometric CO oxidation (cf. Fig. 2). (For interpretation of the references to colour in this figure legend, the reader is referred to the web version of this article).

Table 2
Light-off temperatures of CO, hydrocarbons and NO in stoichiometric TWC feed with either propene or propane as unburned hydrocarbon, and of CO from individual CO oxidation and from TWC feed without hydrocarbon.

Catalyst	Light-off temperature (T_{50}), K[a]							
	... of CO				... of hydrocarbon		... of NO	
	CO $+O_2$[b]	CO + NO $+O_2$[c]	Propane[d]	Propene[d,e]	Propane[d]	Propene[d,e]	Propane[d]	Propene[d,e]
Au/Al_2O_3	427	472	536	706	> 750	706	–	–
$Au/La\text{-}Al_2O_3$	< 320[e]	417	417	583	> 750	625	–	–
$Au/CeZrO_x$	385[e]	396	432	468	> 750	552	–	–

[a] Temperature of 50% conversion of the reactant.
[b] CO (1.1%), O_2 (0.55%), balance He.
[c] CO (1.1%), NO (0.1%), O_2 (0.5%), balance He.
[d] Hydrocarbon in TWC model feed, for composition see Section 2.3.
[e] from Ref. [8].

with propane representing the hydrocarbon was much poorer even than with propene [8]. Although CO conversion happened at lower temperatures, the hydrocarbon was almost not converted at all and NO was less converted than with propene, the reaction product being mostly the undesired N_2O. However, as indicated in Ref. [15], the unburned hydrocarbons are mostly unsaturated in reality, therefore, propene is certainly a more appropriate model for them.

3.2.2. *Influence of third components on CO oxidation*

In Figs. 2 and 3, we present conversion curves measured during CO oxidation in the presence of third components. During these experiments, we noted differences between first and second runs while changes in further runs were marginal. These stabilization (or formation) phenomena will be briefly reviewed first.

CO conversion curves over fresh Au/Al_2O_3 are compared with those of the second run in Fig. 2a. With the fresh catalyst, a curve exhibiting a minimum below 500 K before full conversion was reached at ca. 600 K was obtained in the binary feed. Conversion curves with a minimum, which were categorized as “smiling” or “camel-like” [16,17] were reported in several studies of CO oxidation over supported gold [16–22]. Notably, this “smile” was observed also in the presence of NO or of both NO and propane, although conversions were strongly suppressed by the additional components similar as in the second runs (Fig. 2a). Although different reasons for such feature were proposed in literature, we have not attempted to elucidate the mechanism underlying the present one because it is out of our focus on hydrocarbon influence on three-way catalysis. In our case, the feature might be due to irreversible changes in metal-support interaction during operation at higher temperatures. It was strongly suppressed after the 1st run, leaving the catalyst considerably deactivated except for the HC off feed where the effect depends on the temperature range considered (Fig. 2a).

On the remaining supports, gold did not exhibit similar changes between first and second CO oxidation run (Fig. S2), therefore, we did not search for such effects in the presence of hydrocarbons. However, another formation process occurred in the presence of NO (i.e., the HC-off feed containing NO together with CO and O_2). The data are reported in a similar format in Fig. 2b and c. They show that interaction with this feed activated the catalysts, though to a different extent depending on the support: drastically for $Au/La\text{-}Al_2O_3$ and significantly for $Au/CeZrO_x$. In the case of Au/Al_2O_3, the curves of which have been repeated from Fig. 2a, the probably thermal deactivation described above and the activation by interaction with the NO containing feed appeared to be superimposed. We presume that such activation in the presence of NO might be due to nitrates forming near the active sites, but we cannot provide evidence for this assumption so far.

In these experiments, NO conversion exhibited a complex behavior, significantly different from the performance in reaction atmospheres containing hydrocarbons. In the first runs, significant conversion was

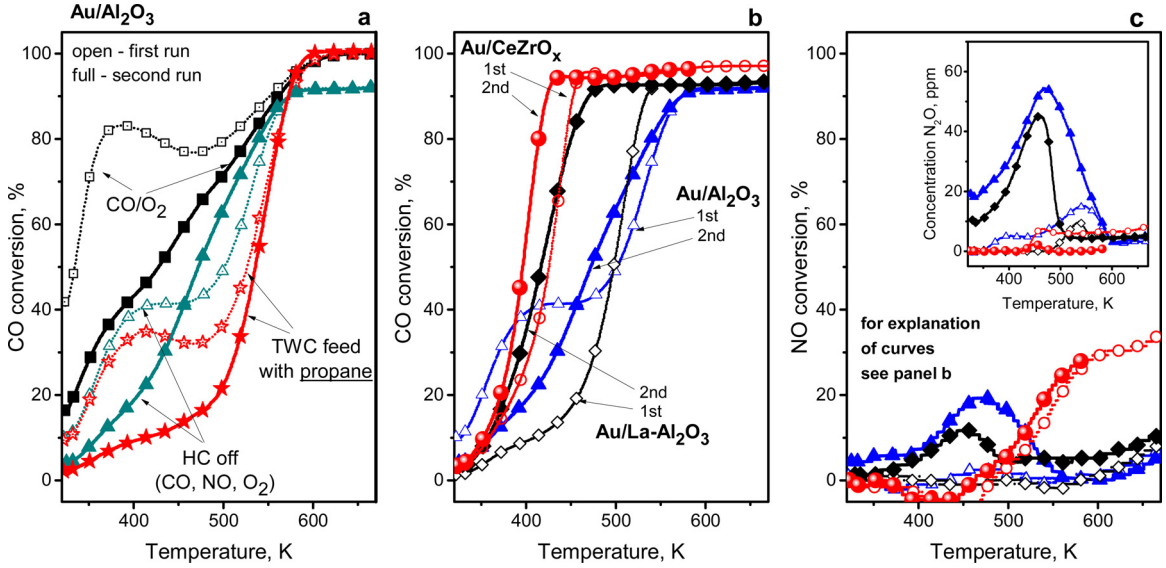

Fig. 2. Stabilization of supported Au catalysts during use in reactions related to three-way catalysis a) CO conversion in presence of co-reactants during 1st (open symbols) and 2nd run (full symbols) over Au/Al_2O_3; CO (b) and NO (c) conversions in the "HC-off" feed (CO, O_2, NO) in the 1st and 2nd run, N_2O formation is displayed as an inset in c). After 2nd run further changes were marginal.

observed only over $Au/CeZrO_x$ (Fig. 2c). In the second run, NO conversion peaked below 20% at 473 K over Au/Al_2O_3, apparently due to N_2O formation (inset of Fig. 2c). In the presence of propane, this feature was completely poisoned (Fig. 1c). Likewise, conversion of NO by CO to largely N_2 over $Au/CeZrO_x$, which started above 500 K both in the first and second run (Fig. 2c), was replaced by some NO conversion with propane around 500 K (cf. Fig. 1b, c). Over $Au/La\text{-}Al_2O_3$, NO conversion peaks around 470 K were obtained in both feeds, in agreement with the view that this results from a NO/CO reaction (see above). The peak was, however, somewhat higher in the propane-containing feed, which may suggest some involvement of the hydrocarbon. In the TWC feed containing propene, the low-temperature features over the alumina-based catalysts (Fig. 2c) were completely poisoned, NO conversion started above 500 K only (Fig. 4 in Ref [8].). Over $Au/CeZrO_x$, the onset of NO conversion in this feed [8] was very similar to that in the "HC-off" mixture (Fig. 2c). However, the extent of N_2O formation was much more extensive in the presence of propene [8], thus, surface processes appear to be changed by the hydrocarbon also in this case.

In Fig. 3, CO conversion curves in TWC feeds with propene and propane are compared with curves measured in feeds with one or more components missing. CO oxidation was suppressed on all catalysts by adding the components of the TWC mixture. Interactions between components have been examined in most detail with Au/Al_2O_3 (Fig. 3a). In the low-temperature region (up to 350 K), CO oxidation was poisoned by any of the added components to a similar extent, which is similar to what has been reported by Bauer et al. for Au-CuO/SiO_2 catalysts recently [23]. Above 350 K, the conversion curves with NO or propane added to the binary feed were very similar over Au/Al_2O_3 (Fig. 3a), which may suggest that NO and propane compete with CO for adsorption on the active sites with similar efficiency. In the presence of both components together (TWC feed with propane), the CO conversion curve increased much more slowly. Apparently, propane and NO interact at the active sites thus enhancing the poisoning. Propene was a much stronger poison already alone, which confirms the particular poisoning effect of the double bond as proposed earlier [8]. Without NO in the feed, CO conversion remained virtually zero and

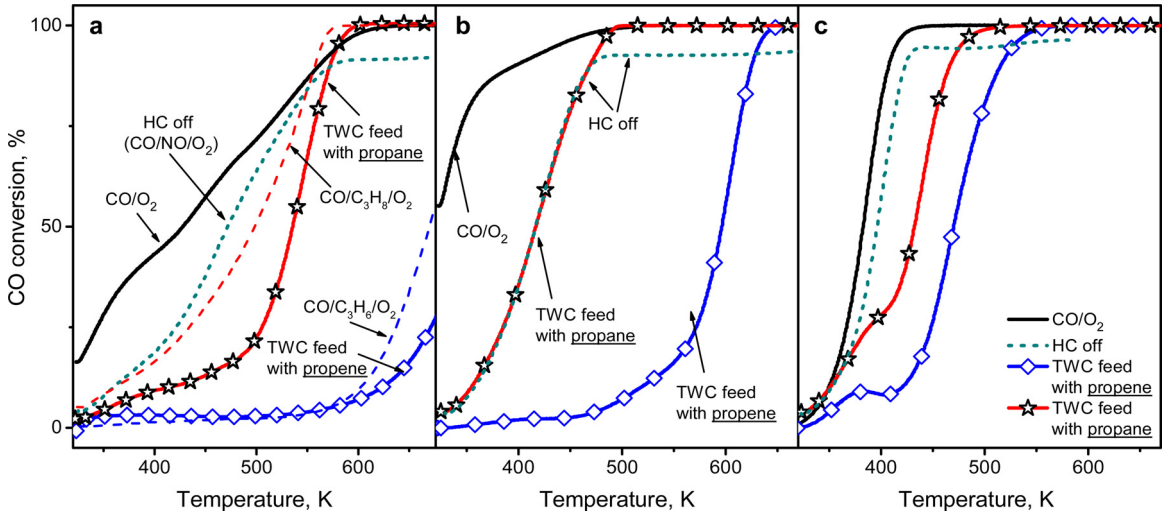

Fig. 3. Influence of third components on CO oxidation over supported Au catalysts. CO conversions in binary feed and in three-way catalysis model feeds containing propane, propene, or no hydrocarbon, a – Au/Al_2O_3, showing additionally curves for CO oxidation in presence of propene and propane, b – $Au/La\text{-}Al_2O_3$, c – $Au/CeZrO_x$.

took off only above 600 K, but in the presence of NO, even this take-off was delayed. Here, we note significant differences to the data reported for Au-CuO/SiO_2 [23], which behaved very similar in CO oxidation with only NO or with propene (or NO + propene) added.

The general comparison shows, however, that the responses of the catalysts to additional components depended on the supports (Fig. 3). As to CO oxidation in binary feed, Au/La-Al_2O_3 clearly outperformed Au/$CeZrO_x$ in the low-temperature range, but at high conversions further increase was significantly delayed (Fig. 3b, c). Au/$CeZrO_x$ started at just 2% conversion at 323 K (Au/Al_2O_3 – 15%), but while the alumina-supported Au took off very slowly reaching full conversion only around 600 K (Fig. 3a), Au/$CeZrO_x$ achieved this already around 400 K (Fig. 3c). With the remaining components added, strong poisoning effects were noted in particular for Au/La-Al_2O_3 (Fig. 3b). At 350 K, CO conversions were in the same range around 10% over all catalysts in all feeds except for the binary ones.

Beyond 350 K, CO conversion curves in the three feeds (HC-off, TWC/propene and -/propane) took very different courses. Those in TWC/propene feed were suppressed most drastically, but were on the other hand most obviously influenced by the reducibility of the supports as described earlier [8]. Inhibiting effects of propene on CO oxidation including their mitigation by a $CeZrO_x$ support as compared to Al_2O_3 have been recently reported also for supported Pd catalysts [24]. The effect observed with our gold-based systems seems, however, stronger. Such intense interaction with propene would be expected for an acidic rather than for a metal site. It has been pointed out that cationic Au^I is a strong Lewis acid [25–28], but from our XPS [8] and XAFS [29] work we have no evidence that Au^I might be available in our catalysts. On the other hand, fully reduced alumina-supported gold has been reported to be a brilliant catalyst for a reaction observed so far only on acidic catalysts (α-pinene isomerization [30]). The strong differences between the impacts of propane and propene on Au-catalyzed CO oxidation tend to support the idea that supported gold may be able to engage in acid-base interactions.

When propene was replaced by propane, CO conversions generally exhibited the well-known S-shape resulting from the kinetics of a single reaction. Compared with Au/La-Al_2O_3 (Fig. 3b), the onset of the steep section was delayed by a slow linear increase over Au/Al_2O_3 (Fig. 3a), and by a shorter, but rather steep linear section over Au/$CeZrO_x$ (Fig. 3c). As a result, the light-off temperature of CO oxidation in the propane-containing mixture was slightly lower over Au/La-Al_2O_3 than over Au/$CeZrO_x$ (Table 2). In the relations between CO conversions in TWC/propane and HC-off feeds, there was no clear trend. Over Au/Al_2O_3 and Au/$CeZrO_x$ (Fig. 3a, c), CO conversions in presence of propane clearly lagged behind those in the absence of hydrocarbons while there was no difference at all over Au/La-Al_2O_3 (Fig. 3b). Taking into account that the HC-off feed contains significantly less oxygen (cf. Section 2.3) one might still state a higher reactivity of the Au/La-Al_2O_3 catalyst in this feed but, the differences are much smaller than with the other catalysts. The strong impact of the supports on the temperature dependence of these poisoning phenomena suggests that the sites on which the interaction with the third component takes place are at the perimeter between gold and the support.

3.2.3. Removal of deposits by gas-phase oxygen

The differences in the extent of propene poisoning on supports of different reducibility were earlier assigned by us to the effect of active support oxygen preventing the formation of deposits on the active metal sites [8]. The presence of deposits on our catalysts was examined by TPO and TG. TPO profiles for released CO_2, CO, and N_2O are shown in Figs. 4 and S3, and the amounts of the components detected are reported in Table 3. CO_2 was always the major product, the quantity of CO released being more than an order of magnitude less. Nitrogen-containing molecules were detected as well though in very small quantities. The N_2O profile was sufficiently intense to be quantified with the IR detector used, while that of NO was not. NO could be, however, quantified by mass spectrometry in the TG measurements summarized below (cf. Fig. S4) where N_2O was superimposed by the CO_2 signal.

TPO curves were measured also with the bare supports (Fig. 4). They exhibit one broad peak for both CO_2 and CO, with a pronounced maximum between 730 and 790 K. At lower temperatures a significant CO_2 peak was observed at 490 K for $CeZrO_x$, but also from La-Al_2O_3, and even from Al_2O_3 some CO_2 was released already between 500 and 600 K, hardly beyond detection limits in the latter case. N_2O was not detected in significant amounts.

On the supported Au catalysts, deposits were formed in larger quantities (cf. Table 3). Generally, combustion started at lower temperatures than in the absence of gold, but the first peak at ≈400 K was obtained from Au on $CeZrO_x$ and on La-Al_2O_3 only. On the other hand, these catalysts differed strongly in the extension of the signal of CO_2: while its concentration returned to near zero below 700 K in the case of Au/$CeZrO_x$, it produced a significant maximum at ≈740 K in the case of Au/La-Al_2O_3, and a pronounced peak in the case of Au/Al_2O_3 where the leading feature at ≈400 K was completely absent. In the high-temperature region, the decay of the CO_2 signals from the Al_2O_3-based samples was very similar irrespective of the presence or absence of gold (Fig. 4). On the contrary, the pronounced peak at 790 K desorbing from pure $CeZrO_x$ had completely disappeared in the presence of gold. Regarding CO, it is safe to state that quantities released were largest from (Au)/Al_2O_3 and smallest from (Au)/$CeZrO_x$, despite some uncertainty due to the small concentrations (Table 3). Quantities released in the presence of gold were generally smaller than in the absence of gold, which is highly active for CO oxidation.

In Fig. S3, data for Au/$CeZrO_x$ and Au/Al_2O_3 after contact with TWC/propene feed are compared with those given in Fig. 4, which refer to the state after the feed variation experiment (cf. Section 2.3, Fig. S1). As expected, more CO_2 than after final contact with HC-off feed was released from Au/Al_2O_3 (cf. Table 3) where the two features at 630 K and 730 K grew higher than after exposure to HC-off feed. In the profile Au/$CeZrO_x$ poisoned in TWC/propene feed at 523 K (Fig. S3), the leading feature at ≈400 K appeared almost unchanged as compared with the state after contact with HC-off feed (Fig. 4), but it was followed by a pronounced peak at 530 K, which decayed to very small values up to 700 K. From this catalyst, a TPO analysis was also made after exposure to TWC feed at 673 K, which does not deactivate the catalyst at all (cf. Fig. 3c). The profile, which is shown with an offset in Fig. S3, is very close to that after exposure to the HC-off feed, and the quantity of CO_2 released was the same (Table 3).

Deposits remaining after the feed variation experiment (i.e. the state before TPO as shown in Fig. 4) were also examined by TG/MS, and results are summarized in Fig. S4. As the weight data include the release of water, which was not quantified in the TPO experiment, comparison makes sense only for the data from product analysis (Fig. S4b, Fig. 4). The major differences between the experiments are the stagnant gas phase in the TG crucible vs. forced flow through the bed in TPO, and the oxygen content in the gas phase (20% in TG, 5% in TPO). The latter may be the reason why CO was not detected in the TG effluent.

Generally, CO_2 profiles from TG are quite similar to those from TPO. Closer examination shows that the latter extend to higher temperatures and that those from TG are more intense at lower temperatures. In the case of Au/Al_2O_3, some CO_2 release can be detected already below 400 K, and the low-temperature shoulder in TPO has become the main peak in TG, followed by a high-temperature shoulder. Likewise, the CO_2 profile from Au/La-Al_2O_3 has an increasing tendency in TPO, but a decreasing trend in TG, and the minor shoulder at 500 K in the TPO profile from Au/$CeZrO_x$ is missing in the TG profile. Such differences can be assigned to the different oxygen content and flow pattern of the gas phase.

The desorption of nitrogen oxides, though in low quantities, is a remarkable result of our study on the deposits. From Au/Al_2O_3, desorption of both N_2O and NO could be detected in the whole temperature

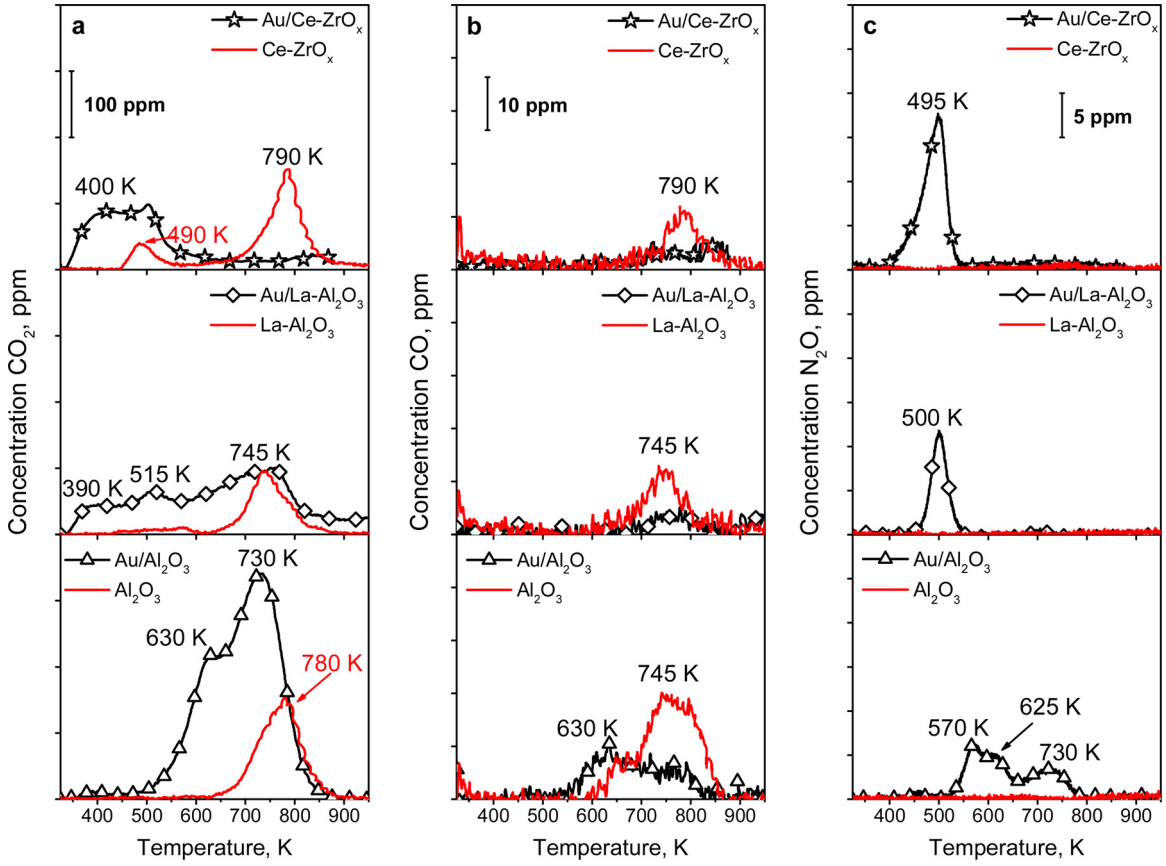

Fig. 4. Formation of CO_2 (a), CO (b), and N_2O (c) from Au/$CeZrO_x$, Au/La-Al_2O_3, Au/Al_2O_3, and the Au-free supports during TPO experiments in 5% O_2/He performed after the 2nd run in the feed variation experiment (for results – s. Fig. 6).

Table 3
Amounts of CO_2, CO, and N_2O recovered in temperature-programmed oxidation of bare supports and Au catalysts after the feed-variation experiment at 673 K (cf. Fig. 6) and after different treatments.

Catalyst	n(compound), μmol g_{cat}^{-1}			
	n(CO_2)	n(CO)	n($CO_{x,\ total}$)	n(N_2O)
Au/Al_2O_3	312.5	8.5	321.0	4.7
Al_2O_3	84.5	17.0	101.5	0.7
Au/Al_2O_3, TWC feed[a]	432.0	11.0	443.0	5.3
Au/La-Al_2O_3	174.0	4.0	178.0	2.2
La-Al_2O_3	58.0	11.0	69.0	0.4
Au/$CeZrO_x$	102.0	4.0	106.0	6.3
$CeZrO_x$	86.0	6.0	92.0	0.8
Au/$CeZrO_x$, TWC feed[a]	102.0	8.0	110.0	0.6
Au/$CeZrO_x$, TWC feed[b]	137.0	4.5	141.5	1.9

[a] After two runs of feed variation experiment, the second stopped after TWC feed at 673 K for 20 min.
[b] As footnote a, but at 523 K.

range while from Au/$CeZrO_x$ and Au/La-Al_2O_3, N_2O was released only at low temperatures (Fig. 4) but NO at high temperatures (Fig. S4). The comparison of different states of Au/$CeZrO_x$ (Fig. S3, Table 3) sheds some light on the origin of the nitrogen. After deactivation in TWC/propene feed at 523 K, 1.9 μmol g^{-1} N_2O was desorbed below 600 K (cf. Fig. S3). After the catalyst had been regenerated by use in TWC/propene feed at 673 K, less N_2O was released as expected, but when it was regenerated by HC-off feed instead, the most intense N_2O signal was obtained (Table 3). Apparently, the deposits are reactive towards NO: if they are contacted with the HC-off feed at 673 K for activation (see below, Fig. 6), more nitrogen is captured in the hydrocarbon-free environment. This resulted in the unexpected observation that the hydrocarbon load of the catalyst decreased while the nitrogen content in the deposits increased (Fig. S3, Table 3). On the other hand, it agrees with an observation presented below according to which the deposits are the best reducing agents for NO over our catalysts (Section 3.2.5)

The data presented above feature strong differences among the supports involved, in particular between $CeZrO_x$ and Al_2O_3, while La-Al_2O_3 exhibits an intermediate behavior. Deposits gasified at temperatures as low as 400 K are apparently close to gold. However, the example of Au/Al_2O_3 (Fig. 4) shows that such proximity is not sufficient to start combustion at such low temperature. Most likely, active oxygen from the support, which is not available on unmodified alumina, is also required. It appears that surface La oxide species can also provide active oxygen, most likely not by a change of the cation redox state as in case of Ce, but leaving behind oxygen vacancies with electrons trapped (preferably F^+ sites holding one electron) as discussed in Ref. [31] for crystalline La_2O_3. Peaks above 750 K, which are typical of the bare supports, apparently arise from regions far from gold. Such peak was not obtained from Au/$CeZrO_x$. It is, however, difficult to decide if this is just due to the smaller BET surface area of this support (cf. Table 1) and a resulting higher areal density of the Au particles on it or to an activation of surface sections more distant from the gold particles on the more redox active $CeZrO_x$ support.

The significantly higher temperatures required for cleaning the active sites on Au/Al_2O_3, which was observed both by TPO (Fig. 4) and TG (Fig. S4b) agrees with the observation that propene poisoning is most severe with this catalyst (Fig. 3). However, the temperatures of beginning deposit combustion in the O_2/He feed (Fig. 4) were much lower than those where the active sites become available for CO oxidation in the TWC feed (Fig. 3). In addition, according to Fig. 4, one would expect the rise of CO conversion in the model feed in a similar temperature range for both Au/$CeZrO_x$ and Au/La-Al_2O_3, which is definitely not

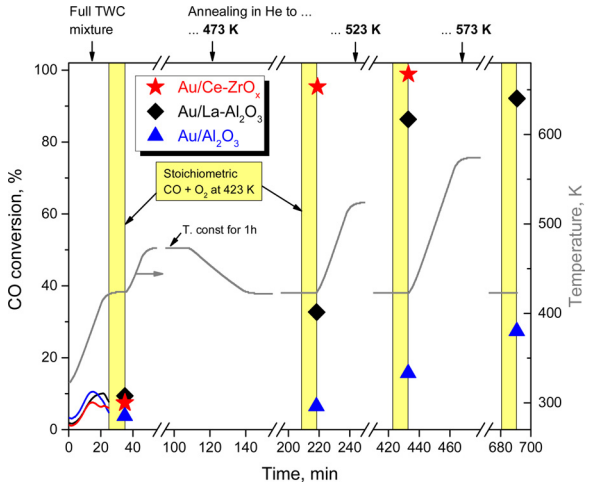

Fig. 5. Regeneration of CO oxidation activity of poisoned supported Au catalysts by annealing in He at different temperatures (473 K, 523 K and 573 K).

the case (cf. Fig. 3b, c). Apparently, experiments in the presence of high oxygen concentrations can demonstrate the existence of deposits and the involvement of nitrogen in them, but are misleading with respect to their removal in TWC feeds with very low oxygen partial pressures.

3.2.4. Removal of deposits by support oxygen

To better approach conditions in the stoichiometric model feeds we examined the course of regeneration by mere heating the catalysts in inert gas where only support oxygen is available for the combustion of deposits. Alternatively, deposits might compact at high temperatures releasing thus some of the active sites. The extent of regeneration has been probed by CO oxidation in the binary feed under mild conditions (423 K, cf. Section 2.3.). Results are summarized in Fig. 5 and in more detail in Table S1.

The catalysts were pretreated by raising the temperature in TWC/propene feed just until 423 K, after which poisoning was confirmed by the low CO conversions in the binary feed (< 10%, Fig. 5). After annealing in He at 473 K, the regeneration effect indicated by the probe reaction was small for Au/Al$_2$O$_3$ (CO conversion increasing from 4% to 7%), significant for Au/La-Al$_2$O$_3$ (9% → 33%) and nearly complete for Au/CeZrO$_x$ (8% → 95%). For the latter catalyst, an intermediate regeneration temperature of 448 K was tried in an extra run, which resulted in a CO conversion of 56% in the binary feed. With all three catalysts, CO conversions after annealing the poisoned samples in He at higher temperatures (523 K, 573 K) confirmed the tendencies of the

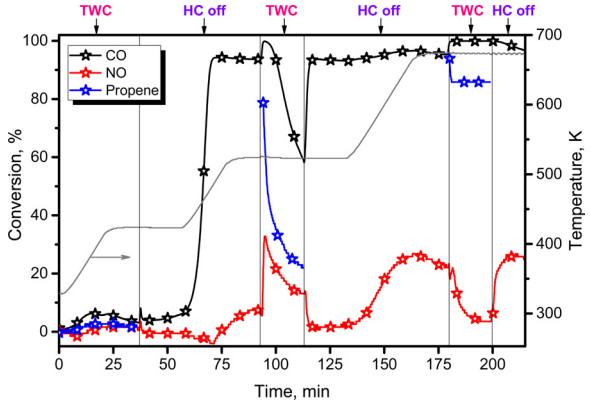

Fig. 6. Regeneration of catalytic activity of Au/CeZrO$_x$ by exposure to hydrocarbon-free feed. All feeds stoichiometric: TWC feed – 1.1% CO, 0.1% NO, 0.1% propene, 0.95% O$_2$, balance He, HC-off feed - 1.1% CO, 0.1% NO, 0.5% O$_2$, balance He.

regeneration effect suggested by the 473 K run (Fig. 5, Table S1). After a final phase at 623 K (not shown in Fig. 5), Au/Al$_2$O$_3$ achieved a CO conversion in binary feed of 41%, still below the 48% expected from the data in Fig. 3a.

In catalysts containing Au deposited on "active" supports, lattice oxygen adjacent to the gold particles has been shown to take part even in the extremely fast CO oxidation [32,33]. CeZrO$_x$ is definitely an active support, therefore, the relatively poor performance of Au on CeZrO$_x$ in the binary feed (Fig. 3c) was surprising (for an explanation proposed by us see section 3.2.6). The easy recovery of its CO oxidation activity (Fig. 5) suggests that the deposits can be indeed oxidized by surface oxygen at a relatively low temperature. Likewise, CO conversion in the full TWC model feed starts at rather low temperature as well (Fig. 3c) because deposits (or their precursors) become oxidized by surface oxygen. On "inert" supports like alumina, active surface oxygen is missing. Indeed, although some regeneration was noted also with Au/Al$_2$O$_3$, CO conversion in the binary feed fell short of the achievable ≈50% (cf. Fig. 3a) even after annealing at 623 K. As in the TPO and TG experiments, Au/La-Al$_2$O$_3$ is again an intermediate case: it was almost completely regenerated at 573 K (Fig. 5, Table S1). As this can be explained only by donation of surface oxygen originally associated to La, the gold particles must be close to La sites. Given the relatively low surface concentration of La (La/Al surface ratio by XPS – 0.013 [8]), this suggests a preferential interaction of Au with the La species during preparation as already mentioned in our previous paper [8].

3.2.5. Identification of reaction paths by transient experiments ("feed variation")

Figs. 6 and S5 report experiments involving switches between feeds of different composition. In the experiment with Au/Al$_2$O$_3$ summarized in Fig. 6, TWC/propene was replaced by HC-off feed and vice versa (see also Fig. S1), originally aiming to examine regeneration by avoiding propene in the feed. The companion experiments with the other two catalysts are shown in Fig. S5.

After interaction with TWC feed at 423 K, all catalysts were inactive also in the HC-off feed (Fig. 6, S5) where CO conversions between 30 and 90% would have been expected (Fig. 3). With Au/CeZrO$_x$, CO conversion took off drastically upon temperature increase, reaching its peak value (≈90% due to unavailability of O from NO) at ca. 490 K. After switching back to TWC feed at 523 K, CO conversion briefly touched 100% before going on decay. The more remarkable result is, however, a jump in NO conversion and a very high onset of propene conversion, which both fell to much lower values subsequently due to the poisoning influence of the hydrocarbon. The duration of this decay (20 min) shows that the high transient propene and NO conversions did not arise from a reaction of propene with adsorbates trapped on the surface. Rather, they are steady-state conversions, though in states subjected to gradual poisoning. Hence, the result of this switch from HC-off to TWC feed suggests that NO is better reduced by propene than by CO around 523 K.

After returning to HC-off feed (113th min), CO conversion jumped to 90% and increased somewhat during the next temperature ramp, which resulted in a NO conversion of ≈25%. Upon the following switch to TWC feed, now at 673 K, NO conversion dropped without an intermediate peak while CO conversion went up to 100% at a stable propene conversion of ≈85%. Apparently, propene was no more available for NO reduction at this temperature and lost competition for gas-phase O$_2$ to CO. The final switch to HC-off feed shows that NO can actually be reduced by CO at 673 K if there is no "excess" oxygen. In the TWC feed, such "excess oxygen" is available to CO because it binds oxygen "assigned for" propene.

The data obtained with the remaining two catalysts is similar except for the higher temperatures required for regeneration. In the case of Au/La-Al$_2$O$_3$ (Fig. S5a), this resulted in a more gradual recovery of activity in HC-off feed during the temperature ramp, with nearly full CO conversion achieved only at 523 K. With Au/Al$_2$O$_3$, this recovery

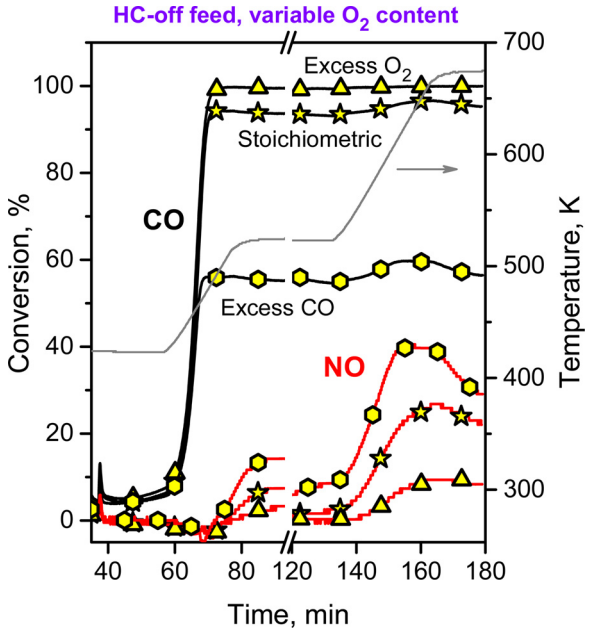

Fig. 7. Competition of O_2 and NO for CO over Au/CeZrO$_x$ at different temperatures. HC-off feed – 1.1% CO, 0.1% NO, O_2 – 0.55% (excess O_2), 0.5% (stoichiometric), or 0.3% (excess CO), balance He.

happened only during the next temperature ramp (Fig. S5b). During the switch from HC-off to TWC feed at 673 K, Au/La-Al_2O_3 produced only very narrow peaks of NO and propene conversion (Fig. S5a), which probably arise from mere changes of surface coverages. Au/Al_2O_3, however, produced long transients with pronounced peaks of NO and propene conversion (Fig. S5b), similar as Au/CeZrO$_x$ upon the same switch at 523 K (Fig. 6). Under steady state, Au/Al_2O_3 was still fully poisoned at 673 K (Fig. 3a) while Au/CeZrO$_x$, which had been poisoned at 523 K, achieved full CO conversion at 673 K (Fig. 3c). While the high propene conversions observed during these transients (Au/Al_2O_3 at 673 K, Au/CeZrO$_x$ at 523 K) certainly reflect the deposition of "coke" on the catalyst surface, the simultaneous NO conversion peaks suggest that intermediates of this coke deposition are actually the reductants for NO. This is supported by the observation that NO can be reduced by propene over Au/Al_2O_3 at 673 K (Fig. S5b), but not over Au/CeZrO$_x$ at the same temperature, where the coke precursors are cleaned off by active support oxygen (Fig. 6).

The strong differences in the reactivity of NO and O_2 for CO are nicely illustrated by an experiment where CO was reacted with these oxidants in different proportions over Au/CeZrO$_x$ (Fig. 7). At 523 K, NO was hardly affected by CO, and NO conversion remained below 20% even under significant CO excess. At 673 K, NO conversion achieved 40% in this feed. Notably, catalyst deactivation was observed even in these feeds, rather fast in excess CO, but also in stoichiometric feed (see gap between 80 and 120 min time on stream). The reason for this has not been found out. It is, however, remarkable that the HC-off feed, which was successfully used to remove propene poisoning, caused deactivation of the catalyst itself. IR studies in the presence of an atmosphere containing NO, also together with other components, which were beyond the scope of the present work, may elucidate the reasons for this in the future.

3.2.6. IR studies

Results of our DRIFTS investigation of CO adsorption and CO/propene co-adsorption on supported Au catalysts are shown in Figs. 8 and 9. During CO adsorption at room temperature (Fig. 8a, b), changes relative to the clean catalyst surface occur in three regions: between 1800 and 1200 cm^{-1}, which is a range typical of surface carbonate and formate species, in the region indicating adsorption of CO at metal or support sites (2300-1900 cm^{-1}), and in the OH region from 3800 to 3500 cm^{-1}. The OH and carbonate regions exhibit very different signals on the two supports, in the OH region, negative intensity is observed.

The overall higher band intensities on Au/CeZrO$_x$ can be related to the higher redox activity of the Ce-containing support, which oxidizes the CO adsorbate. Intense broad and asymmetrical bands centered at ca. 1615 cm^{-1} and at ≈1300 cm^{-1} accompanied by narrow signals at 1394 and at 1219 cm^{-1} result from this interaction (Fig. 8a). According to literature, these signals might arise from hydrogen carbonates, mono-, bi-, and polydentate carbonates and formate species ([34], cf. detailed assignment in Table S2). The formation of hydrogen carbonate species is accompanied by the development of their ν(OH) vibration at 3620 cm^{-1} at the expense of different types of terminal isolated OH groups (originally at 3752 and 3728 cm^{-1}), which causes negative intensities. At the same time, contributions due to bridging isolated hydroxyl groups at ≈3690 cm^{-1} increase. The formation of formate species is indicated by decreasing intensity of bridging isolated OH groups at the Au/CeZrO$_x$ interface at ≈3658 cm^{-1} [34]. A very weak and broad signal at ≈2860 cm^{-1}, which can be hardly discerned at the present scaling, might arise from the ν(CH) mode of formate species [35].

The much weaker carbonate signals on Au/La-Al_2O_3 (Fig. 8b) consist of a broad asymmetric feature peaking at 1658 cm^{-1} with a pronounced shoulder at 1616 cm^{-1} and a narrow weak signal at 1433 cm^{-1} together with a very weak signal at 1398 cm^{-1} (Fig. 8b). These signals can be distinctly assigned to different types of hydrogen carbonate species [36], but they might be superimposed by contributions of mono- and bidentate carbonates. In addition, band widths indicate a strong heterogeneity of the basic surface sites. At the same time, signals expected for the ν(OH) and δ(OH) modes of the hydrogen carbonate species (≈3620 and 1228 cm^{-1}) are very weak. We believe that this results from interactions of hydrogen carbonate OH groups with alumina surface OH groups [37], which should be still abundant after the mild treatment applied to our sample. Actually, the interpretation of the OH region is challenging for both supports, probably due to rather high initial hydroxylation degrees. However, hydrogen carbonate formation involves surface OH groups, which might affect the vibrational frequencies of adjacent OH groups. Moreover, the consumption of surface oxygen during carbonate formation, be it by reduction of the associated Ce^{4+} cation to Ce^{3+} (CeZrO$_x$) or by the creation of nearby oxygen vacancies (La-Al_2O_3), might influence the surface hydroxyl groups as well.

In our spectra, the CO region is superimposed by the rotational structure of the gas-phase CO signal (cf. dip between P and R branches at ca. 2140 cm^{-1}), but major adsorbed species can be still observed. On Au/CeZrO$_x$ (Fig. 8a), a signal appeared at 2112 cm^{-1} upon exposure to 0.5 mbar CO and shifted to 2104 cm^{-1} with increasing CO pressure. Signals in this range are usually assigned to CO at the perimeter of neutral Au metal nanoparticles and (reducible) supports like TiO_2 or CeO_2 [38–41]. In the interaction of CO with group 11 metals, where back-donation from the metal into the CO 2π* orbital is relatively weak, bonding is dominated by the weakly antibonding 5σ orbital donating electrons to the metal. Growing CO coverage therefore increases the electron density at the metal site, which results in enhanced π back-donation and red-shifts of the CO signal [42]. On supported Au catalysts, bands of CO coordinated to perimeter sites of positively charged Au clusters ($(Au)_n^{\delta+}$) and to exposed support cations are often found around 2125 cm^{-1} and 2160 cm^{-1}, respectively [43,44]. The presence of such sites remains unclear in our case due to the signal of gas-phase CO.

Upon extended exposure to CO at room temperature, the signal of CO on Au perimeter sites was converted to one at even lower wavenumber (2071 cm^{-1}), which was assigned to CO on negatively charged Au sites in literature [45]. The appearance of such a strongly redshifted band indicates a high electron density at the corresponding metal sites due to a metal-support interaction. The electron donating effect might

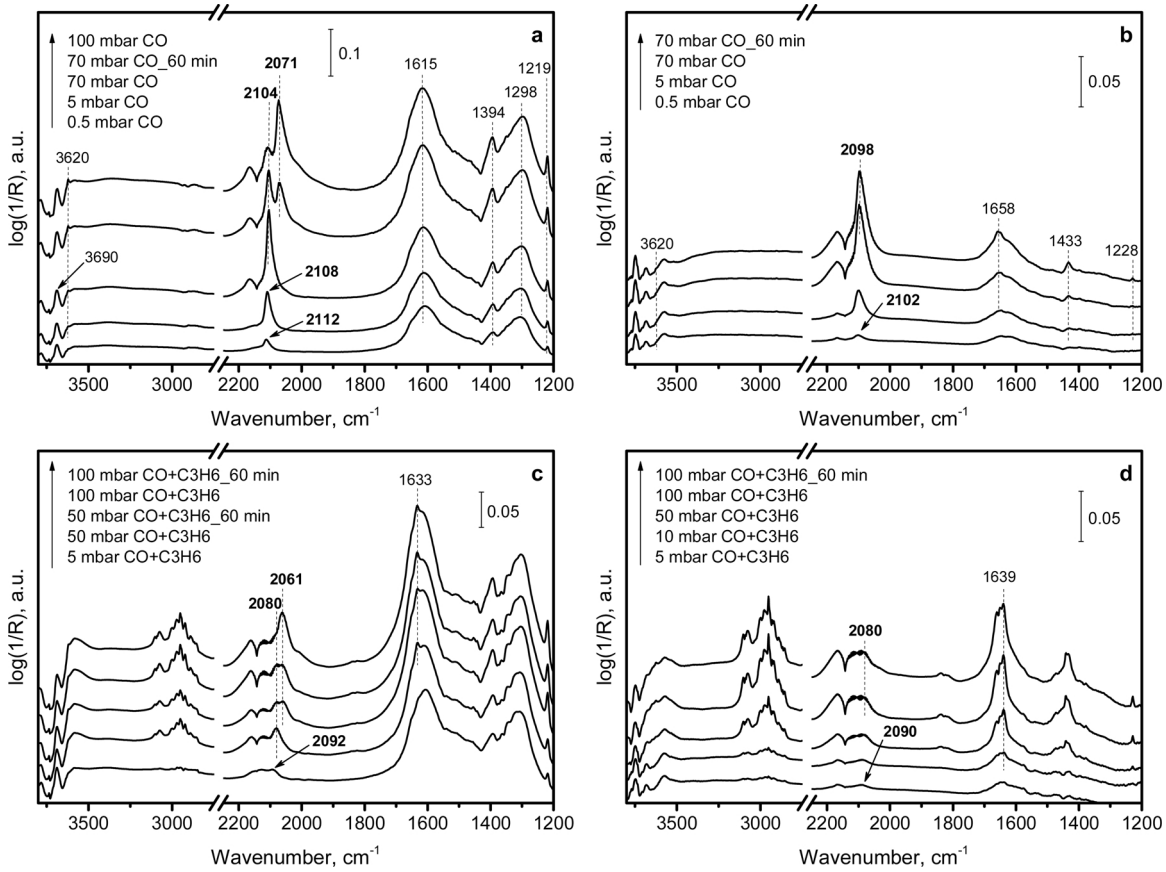

Fig. 8. DRIFT spectra taken during adsorption of CO (a,b), and co-adsorption of CO and propene at a ratio of 9:1 (c,d) at 303 K and different partial pressures on Au/$CeZrO_x$ (a,c) and Au/La-Al_2O_3 (b,d).

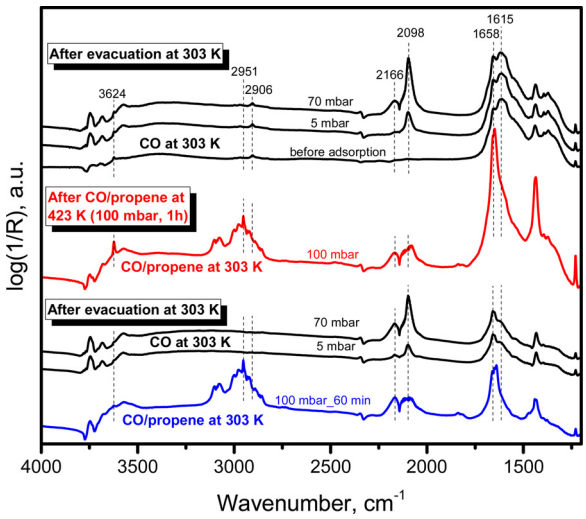

Fig. 9. DRIFT spectra taken during adsorption of CO or co-adsorption of CO and propene at a ratio of 9:1 on Au/La-Al_2O_3 under different conditions including attempted restoration of the surface by evacuation at 303 K. (For interpretation of the references to colour in the text, the reader is referred to the web version of this article.)

result from extensive reduction of surface Ce^{4+} to Ce^{3+} during the experiment. A similar restructuring of a CO absorption band has been reported for Au/CeO_2, though under much more severe conditions (573 K) [46], and accompanied by a shift of the coexisting band of CO on Au° to higher wavenumbers. From the latter, the authors concluded that reduction of the support causes a decrease of the Au particle size, which may not take place under our milder conditions. On Au/La-Al_2O_3, no new band emerged due to surface reconstruction and the band of CO on Au (at 2102 cm^{-1} under 0.5 mbar CO) was redshifted by just 4 cm^{-1} at increased CO coverage (Fig. 8b).

In the presence of propene, the carbonate region on both catalysts exhibited a slightly modified structure (Fig. 8c, d), in particular on Au/La-Al_2O_3. This is at least partly due to signals from gas-phase and adsorbed propene (see detailed assignment on the basis of refs [47,48]. in Table S2). The adsorption of propene was indicated by additional signals at 1633 cm^{-1} on Au/$CeZrO_x$ and at 1639 cm^{-1} on Au/La-Al_2O_3, which are assigned to the ν(C=C) vibrational mode of propene in agreement with recent literature [49]. Coordination of the π electrons of the C=C bond to the surface results in a slight redshift of the ν(C=C) signal relative to that of gas phase propene (1652 cm^{-1}), which is somewhat larger for $CeZrO_x$-supported gold (19 cm^{-1} vs. 13 cm^{-1}). Apparently, these π interactions only slightly affect the electronic structure of propene, which suggests a weak adsorption of molecular nature [49], probably stronger with Au on $CeZrO_x$ than on La-Al_2O_3. In general, however, changes introduced by the addition of propene were smaller in the case of Au/$CeZrO_x$ (compare Fig. 8a, c and b, d) because here the signals in the corresponding wavenumber ranges were more intense already without the hydrocarbon.

In the CO region, dramatic changes were caused by the co-adsorption of propene. Signals of CO on Au° were much weaker and shifted to lower wavenumbers. In the spectrum of Au/$CeZrO_x$, a weak broad signal appeared at 2092 cm^{-1} under 5 mbar gas pressure, while the corresponding signal in pure CO was located at 2108 cm^{-1} under equal CO pressure (Fig. 8c, a). With increasing pressure of the gas mixture, this signal shifted to 2080 cm^{-1} (in pure CO to 2104 cm^{-1}). Again, the signal became reconstructed during extended exposure to elevated pressure, and also the new band appeared redshifted relative to that in

pure CO (2061 cm^{-1} instead of 2071 cm^{-1}). Likewise, the first signal of CO adsorbed on La-Al_2O_3-supported Au° appeared at 2090 cm^{-1} in the presence of propene (instead of 2102 cm^{-1} without propene, Fig. 8d, b). With increasing pressure, this signal also shifted slightly to 2080 cm^{-1} but remained unreconstructed as in the absence of propene. The more pronounced redshifts of the CO absorption bands in case of Au/$CeZrO_x$ during the co-adsorption experiment correlate with the stronger adsorption of propene on this catalyst, which results from stronger electron donation of the propene double bond to the catalyst surface.

With respect to catalysis, the room-temperature conditions applied so far correspond to those where CO oxidation was strongly inhibited by a co-reactant on Au/La-Al_2O_3 and Au/Al_2O_3 (Fig. 3b, a), while conversion was low over Au/$CeZrO_x$ even in the absence of propene (Fig. 3c). The influence of propene alone on CO oxidation rates has been actually demonstrated by us only for Au/Al_2O_3 (Fig. 3a), but the results with other mixtures, e.g. with HC-off (= CO/O_2 + NO, Fig. 3) suggest that the effect would be similar on the other catalysts.

Our IR spectra confirm adsorption competition to be a major reason for the poisoning effect in the low temperature range: bands of adsorbed CO are strongly attenuated, apparently due to the competetive propene adsorption. This would, however, not explain why Au on La-Al_2O_3, which was highly active in the binary feed, was strongly poisoned by the propene while where CO conversion over Au/$CeZrO_x$ was low in this temperature range even without propene (Fig. 3c). We propose that this observation may be also explained on the basis of the redshifts observed with the signal of CO on Au perimeter sites and the increased electron density of Au particles indicated by the very low vibrational frequencies of CO.

Starting with pure CO, we note that the extraordinary activity of Au on reducible oxides, e.g. TiO_2, is often assigned to sites at the perimeter between positively charged Au clusters and the support [18,25], which can be detected on Au/TiO_2 by a signal of adsorbed CO at ≈2125 cm^{-1} [18,43]. The positive charge has been shown to result from an interaction of the small gold cluster with an oxygen vacancy of the TiO_2 surface [50]. Indeed, in earlier work, we found thermal treatment of Au/TiO_2 in inert gas to result in higher activities than activation in air which quenched the above-mentioned IR signal [18]. In the present study, the signal of $Au_n^{\delta+}$ expected at ≈2125 cm^{-1} could not be observed due to the gas-phase contributions (Fig. 8). However, on Au/$CeZrO_x$ the signal of CO at the perimeter of neutral Au particles was observed to redshift with ongoing adsorption, in addition, it was converted to a band typical of CO adsorbed on negatively charged Au clusters [51]. The latter effect is probably due to an extensive reduction of support sites resulting in electron transfer towards Au. Whatever the actual reason, extensive charge transfer towards the Au particles would certainly quench the positive cluster charge, which is assumed to be beneficial for CO oxidation activity. Such extensive redshift of the CO band did not happen with Au on La-Al_2O_3, apparently because La cannot change its oxidation state easily. This confines reduction of the surface oxide phase to the creation of individual defects as in the case of TiO_2.

During CO oxidation, where the CO partial pressure is in the range of 10 mbar only and oxygen is present, reduction processes will be less pronounced than suggested by Fig. 8a and c. But the better stability of La towards overreduction (or its limited tendency to donate electrons) may certainly explain the higher activity of Au on its surface: Combining conversions at 323 K (Fig. 3b, c) with a first-order rate law shows CO oxidation to be 10–20 times faster over Au on this support than on $CeZrO_x$. Such ratio could not arise only from the differences in perimeter lengths resulting from the slightly different particle sizes (Table 1).

Co-adsorption of CO and propene (Fig. 8c, d) resulted not only in the loss of CO band intensity but also in a further redshift due to the electron donating effects of the coordinated C=C bond. The additional electron transfer to gold indicated by this redshift should result in a further loss of CO oxidation activity for sites still accessible to CO. This will be difficult to detect for Au/$CeZrO_x$ where activity is small already without propene, but prominent for the highly active Au/La-Al_2O_3.

Fig. 9 shows selected spectra taken from Au/La-Al_2O_3 with the intention to examine the reason for the particular poisoning effect exerted by propene at elevated temperatures. The lowest spectrum was measured during co-adsorption at room temperature, it repeats the topmost trace in Fig. 8d. After evacuation, the region around 3000 cm^{-1} was flat and the carbonate region had a similar appearance as before. Upon dosing CO, the signal assigned to adsorption at neutral Au particles appeared at 2098 cm^{-1} as on a fresh sample (Fig. 8b). The presence of the gas-phase signal at 2166 cm^{-1} allows for a coarse comparison of coverages. The ratio between heights of the signal at 2098 cm^{-1} and the gas-phase signal was 3.4 both before and after the experiment with propene. Apparently, evacuation restored the CO adsorption sites unchanged.

The specific poisoning effect of propene at higher temperatures was simulated by subjecting the Au/La-Al_2O_3 catalyst to the CO/propene mixture at 423 K. Fig. 9 reports a spectrum measured after this treatment in the same mixture at 303 K (red trace). The appearance of the CO region in this spectrum was much like during CO/propene co-adsorption on the fresh sample (blue trace). Differences were obvious in the carbonate and OH regions. In the latter, a sharp band at 3620 cm^{-1} appeared where previously only a weak unstructured increase of intensity was noted. In the carbonate region, the intensities of all signals related to the vibrational modes of the hydrogen carbonate species were increased and a marked shoulder at ca. 1610 cm^{-1} was observed. After evacuation, the contributions of gas-phase and adsorbed propene were removed (lowest spectrum of top series), except for weak bands at 2906 cm^{-1} and 2951 cm^{-1}. Surprisingly, CO adsorbed on this sample like before the treatment: its band appeared at the same 2098 cm^{-1}, and the height ratio between this band and the gas-phase feature at 2166 cm^{-1} of 3.8 suggests that there was no significant loss of CO chemisorption sites.

For the interpretation of these results, it is important to note that bands around 1600 cm^{-1} are typical of coke deposited on catalyst surfaces. The information is mostly from studies of coking in zeolites. Karge et al. assigned a band at 1610 cm^{-1} as “coke band” [52]. More recently, Castagno et al. ascribed a band at 1590 cm^{-1} to polyaromatic coke while (poly)olefinic deposits were considered to absorb at ≈1620 cm^{-1} [53]. Therefore, the interaction of the CO/propene mixture with the Au/La-Al_2O_3 catalyst at 423 K did not only enhance carbonate formation but resulted also in deposition of carbonaceous residues, which seem to contain still methyl groups (bands around 2900 cm^{-1}). Such “coking” will involve dehydrogenation of oligomers and polymers. Notably, these oligomers/polymers cover the support rather than the metal sites because after removal of propene from the gas phase, CO adsorption was not attenuated.

According to these results, the specific poisoning effect of propene is indeed caused by coke formation, but it is not CO adsorption which is inhibited. It has been pointed out by Behm and coworkers that CO oxidation above room temperature involves active oxygen from reducible supports [33]. Its participation in the reaction mechanism is apparently prevented by the coke. But at increased temperatures, which depend on the redox activity of the support, it burns the deposits and becomes free to engage the oxidation reactions required for three-way catalysis.

4. Conclusions

During CO oxidation over supported Au catalysts in the presence of other components typical of three-way catalysis, two different poisoning phenomena were observed. In the presence of propane, propene, and/or NO, CO oxidation was significantly inhibited below 370 K over Au supported on Al_2O_3 or on La-stabilized Al_2O_3, but not on Au/$CeZrO_x$ where activity was relatively low anywhere. Based on DRIFTS data on (co)adsorption of CO and propene we propose that this poisoning

results from competitive adsorption and operates via two channels. Beyond the simple site blocking, electron transfer from the co-adsorbates towards the active sites, the most active of which are assumed to be at the perimeter of positively charged Au clusters and support according to literature reports, additionally quenches the reaction. At higher temperatures, a different poisoning mechanism operates in propene-containing feeds. Based on studies by TPO, TG, and DRIFTS, this poisoning was ascribed to the formation of carbonaceous residues (coke). Notably, these do not block CO adsorption sites but the support surface around Au clusters, which confirms the view that support oxygen is involved in oxidation catalysis over supported Au catalysts. While this inhibits the CO oxidation mechanism involving active support oxygen, the latter may oxidize the deposits at higher temperatures. This results in self-regeneration phenomena depending on the redox activity of the support, the temperature and the propene content in the feed.

From responses of NO conversion to variations of feed composition, it was concluded that NO is most favorably reduced by intermediates of coke formation from propene. CO can reduce NO as well in certain temperature ranges, but NO reduction activity of Au remains insufficient.

Acknowledgements

We gratefully acknowledge financial support by the German Science Foundation (DFG, Grant No. Gr 1447/24-1), as well as by the Russian Academy of Sciences and Federal Agency of Scientific Organizations (Project No. AAAA-A17-117041710086-6). We also thank Ms. N. Arshadi and Mr. K. Ollegott for their help in performing this study, and Sasol Germany GmbH and Umicore & Co. KG Hanau (Germany) for donations of supports.

Appendix A. Supplementary data

Supplementary material related to this article can be found, in the online version, at doi:https://doi.org/10.1016/j.apcatb.2018.06.063.

References

[1] M.V. Twigg, Appl. Catal. B 70 (2007) 2–15.
[2] F. Haass, H. Fuess, Adv. Eng. Mater. 7 (2005) 899–913.
[3] R.M. Heck, R.J. Farrauto, S.T. Gulati, Catalytic Air Pollution Control: Commercial Technology, 3rd ed., John Wiley & Sons, New York, 2009.
[4] G. Pattrick, E. van der Lingen, C.W. Corti, R.J. Holliday, D.T. Thompson, Top. Catal. 30–31 (2004) 273–279.
[5] M.S. Scurrell, Gold Bull. 50 (2017) 77–84.
[6] Y. Zhang, R.W. Cattrall, I.D. McKelvie, S.D. Kolev, Gold Bull. 44 (2011) 145.
[7] J.R. Mellor, A.N. Palazov, B.S. Grigorova, J.F. Greyling, K. Reddy, M.P. Letsoalo, J.H. Marsh, Catal. Today 72 (2002) 145–156.
[8] V. Ulrich, B. Moroz, I. Sinev, P. Pyriaev, V.I. Bukhtiyarov, W. Grünert, Appl. Catal. B 203 (2017) 572–581.
[9] S. Tsubota, M. Haruta, T. Kobayashi, A. Ueda, Y. Nakahara, Stud. Surf. Sci. Catal. 63 (1991) 695–704.
[10] B.L. Moroz, P.A. Pyrjaev, V.I. Zaikovskii, V.I. Bukhtiyarov, Catal. Today 144 (2009) 292–305.
[11] J. Sirita, S. Phanichphant, F.C. Meunier, Anal. Chem. 79 (2007) 3912–3918.
[12] P. Miquel, P. Granger, N. Jagtap, S. Umbarkar, M. Dongare, C. Dujardin, J. Mol. Catal. A 322 (2010) 90–97.
[13] B.E. Solsona, T. Garcia, C. Jones, S.H. Taylor, A.F. Carley, G.J. Hutchings, Appl. Catal. A 312 (2006) 67–76.
[14] A.C. Gluhoi, B.E. Nieuwenhuys, Catal. Today 119 (2007) 305–310.
[15] E.J. Lox, G. Ertl, H. Knözinger, F. Schüth, J. Weitkamp (Eds.), Handbook of Heterogeneous Catalysis, 2 ed., Wiley-VCH, Weinheim, 2008p. 2274.
[16] A.C. Gluhoi, PhD Thesis, Leiden University, Leiden, 2005.
[17] J.L. Margitfalvi, A. Fási, M. Hegedüs, F. Lónyi, S. Göbölös, N. Bogdanchikova, Catal. Today 72 (2002) 157–169.
[18] W. Grünert, D. Großmann, H. Noei, M.M. Pohl, I. Sinev, A. De Toni, Y. Wang, M. Muhler, Angew. Chem. Int. Ed. 53 (2014) 3245–3249.
[19] Y. Wang, D. Widmann, F. Lehnert, D. Gu, F. Schüth, R.J. Behm, Angew. Chem. Int. Ed. 56 (2017) 9597–9602.
[20] Y. Wang, D. Widmann, M. Wittmann, F. Lehnert, D. Gu, F. Schüth, R.J. Behm, Catal. Sci. Technol. 7 (2017) 4145–4161.
[21] I.V. Tuzovskaya, A.V. Simakov, A.N. Pestryakov, N.E. Bogdanchikova, V.V. Gurin, M.H. Farías, H.J. Tiznado, M. Avalos, Catal. Commun. 8 (2007) 977–980.
[22] A. Simakov, I. Tuzovskaya, A. Pestryakov, N. Bogdanchikova, V. Gurin, M. Avalos, M.H. Farias, Appl. Catal. A 31 (2007) 121–128.
[23] J.C. Bauer, T.J. Toops, Y. Oyola, J.E. Parks Ii, S. Dai, S.H. Overbury, Catal. Today 231 (2014) 15–21.
[24] W. Lang, P. Laing, Y. Cheng, C. Hubbard, M.P. Harold, Appl. Catal. B 218 (2017) 430–442.
[25] G.C. Bond, C. Louis, D.T. Thompson, Catalyis by Gold, Imperial College Press, London, 2006.
[26] E. Rossi, G. Abbiati, M. Dell'Acqua, M. Negrato, A. Paganoni, V. Pirovano, Org. Biomol. Chem. 14 (2016) 6095–6110.
[27] F. Kleinbeck, F.D. Toste, J. Am. Chem. Soc. 131 (2009) 9178–9179.
[28] S.G. Sethofer, S.T. Staben, O.Y. Hung, F.D. Toste, Org. Lett. 10 (2008) 4315–4318.
[29] V. Ulrich, B. Moroz, I. Sinev, V.I. Bukhtiyarov, W. Grünert, to be published.
[30] I.L. Simakova, Y.S. Solkina, B.L. Moroz, O.A. Simakova, S.I. Reshetnikov, I.P. Prosvirin, V.I. Bukhtiyarov, V.N. Parmon, D.Y. Murzin, Appl. Catal. A 385 (2010) 136–143.
[31] S.J. Huang, A.B. Walters, M.A. Vannice, J. Catal. 192 (2000) 29–47.
[32] M.M. Schubert, S. Hackenberg, A.C. van Veen, M. Muhler, V. Plzak, R.J. Behm, J. Catal. 197 (2001) 113–122.
[33] D. Widmann, R.J. Behm, Acc. Chem. Res. 47 (2014) 740–749.
[34] S. Chen, L. Luo, Z. Jiang, W. Huang, ACS Catal. 5 (2015) 1653–1662.
[35] E. Finocchio, M. Daturi, C. Binet, J.C. Lavalley, G. Blanchard, Catal. Today 52 (1999) 53–63.
[36] N.F.P. Ribeiro, F.M.T. Mendes, C.A.C. Perez, M.M.V.M. Souza, M. Schmal, Appl. Catal. A 347 (2008) 62–71.
[37] J. Szanyi, J.H. Kwak, Phys. Chem. Chem. Phys. 16 (2014) 15117–15125.
[38] C. Schilling, C. Hess, Top. Catal. 60 (2017) 131–140.
[39] J.-D. Grunwaldt, M. Maciejewski, O.S. Becker, P. Fabrizioli, A. Baiker, J. Catal. 186 (1999) 458–469.
[40] J.S. Lee, Z. Zhang, X.Y. Deng, D.C. Sorescu, C. Matranga, J.T. Yates, J. Phys. Chem. C 115 (2011) 4163–4167.
[41] M.A.P. Dekkers, M.J. Lippits, B.E. Nieuwenhuys, Catal. Lett. 56 (1998) 195–197.
[42] J. France, P. Hollins, J. Electron. Spectrosc. Relat. Phenom. 64–65 (1993) 251–258.
[43] F. Boccuzzi, A. Chiorino, M. Manzoli, P. Lu, T. Akita, S. Ichikawa, M. Haruta, J. Catal. 202 (2001) 256–267.
[44] M. Manzoli, F. Boccuzzi, A. Chiorino, F. Vindigni, W. Deng, M. Flytzani-Stephanopoulos, J. Catal. 245 (2007) 308–315.
[45] T. Tabakova, F. Boccuzzi, M. Manzoli, D. Andreeva, Appl. Catal. A 252 (2003) 385–397.
[46] F. Romero-Sarria, L.M. Martinez, M.A. Centeno, J.A. Odriozola, J. Phys. Chem. C 111 (2007) 14469–14475.
[47] R.C. Lord, P. Venkateswarlu, J. Opt. Soc. Am. 43 (1953) 1079–1085.
[48] J. Chen, E.A. Pidko, V.V. Ordomsky, T. Verhoeven, E.J.M. Hensen, J.C. Schouten, T.A. Nijhuis, Catal. Sci. Technol. 3 (2013) 3042–3055.
[49] D.M. Driscoll, W. Tang, S.P. Burrows, D.A. Panayotov, M. Neurock, M. McEntee, J.R. Morris, J. Phys. Chem. C 121 (2017) 1683–1689.
[50] M.F. Camellone, J.L. Zhao, L.Y. Jin, Y.M. Wang, M. Muhler, D. Marx, Angew. Chem. Int. Ed. 52 (2013) 5780–5784.
[51] K. Chakarova, M. Mihaylov, S. Ivanova, M.A. Centeno, K. Hadjiivanov, J. Phys. Chem. C 115 (2011) 21273–21282.
[52] H.G. Karge, W. Niessen, H. Bludau, Appl. Catal. A 146 (1996) 339–349.
[53] P. Castano, G. Elordi, M. Olazar, A.T. Aguayo, B. Pawelec, J. Bilbao, Appl. Catal. B 104 (2011) 91–100.